PNAS
www.pnas.org

Supplementary Information for
Phagocytosis and self-destruction break down dendrites of *Drosophila* sensory neurons at distinct steps of Wallerian degeneration.

Hui Ji[1,4], Maria L. Sapar[1,2,4], Ankita Sarkar[1,3], Bei Wang[1], and Chun Han[1*]
[1]Weill Institute for Cell and Molecular Biology and Department of Molecular Biology and Genetics, Cornell University, Ithaca, NY 14853, USA
[2]Current address: New York Stem Cell Foundation, New York, NY 10019, USA
[3]Current address: RHEONIX, INC., Ithaca, NY 14850, USA
[4]These authors contributed equally to this work
[*]Correspondence and Lead Contact: chun.han@cornell.edu

This PDF file includes:

Other supplementary materials for this manuscript include the following:

Videos S1 to S12

SI Methods

Molecular cloning and transgenic flies

ey-Cas9: Three tandem copies of a 211bp *ey* enhancer (corresponding to nucleotides 2577-2787 in GenBank accession number AJ131630) were inserted into XhoI/SalI sites of pENTR11 (Thermo Fisher Scientific). The resulting entry vector was combined with a Cas9 destination vector which is similar to pDEST-APIC-Cas9 (Addgene 121657) but does not contain Inr, MTE, and DPE in the Hsp70 core promoter to generate the pAPIC-ey-Cas9 expression vector through a Gateway LR reaction.

shot-Cas9: A 3851 bp epidermis-specific enhancer (R38F11) of *shot* was amplified from *R38F11-Gal4* genomic DNA using primers ggggACAAGTTTGTACAAAAAAGCAGGCTACGAGGATGCACTCACTC and ggggACCACTTTGTACAAGAAAGCTGGGTAATGCTGCTTGTGGGAAAG. The PCR product was combined with pDONR221 (Thermo Fisher Scientific) to make pENTR-shot through a Gateway BP reaction. pENTR-shot was then combined with a Cas9 destination vector to generate the expression vector pAPIC-shot-Cas9. The Cas9 destination vector is similar to pDEST-APIC-Cas9 (Addgene 121657) but does not contain Inr, MTE, and DPE in the Hsp70 core promoter.

LexAop-myr-tdTom-GFP(1-10): pAPLO-CD4-tdTom (1) was digested by BglII/AscI, blunted, and religated to remove an XbaI site before 13xLexAop2. The resulting construct is called pAPLOm-CD4-tdTom. An myr-GFP fragment was isolated from pJFRC176-10XUAS-rox-dSTOP-rox-myr-GFP (Addgene 32147) by XhoI/XbaI digestion and ligated to XhoI/XbaI sites of pAPLOm-CD4-tdTom to make pAPLO-myr-GFP. pAPLO-myr-GFP was then digested by BamHI/XbaI and subsequently assembled with a tdTom PCR fragment and a GFP(1-10) gBlock fragment (synthesized by IDT) through NEBuilder DNA Assembly to generate pAPLO-myr-tdTom-GFP1-10.

UAS-sGFP(11)x7: A DNA fragment containing GFP(11)x7 was PCR amplified from a gBlock DNA fragment and cloned into Nhe/XbaI sites of pIHEU-sfGFP-LactC1C2 using NEBuilder DNA Assembly. The resulting construct pIHEU-sGFP11x7 inherits the signal peptide sequence from pIHEU-sfGFP-LactC1C2 but removes the sfGFP-LactC1C2 coding sequence.

LexAop-Wld^S: The Wld^S coding sequence was PCR amplified from UAS-Wld^S genomic DNA and cloned into XhoI/XbaI sites of pAPLOm-CD4-tdTom via restriction cloning to make pAPLO-Wld^S.

UAS-ATP8A: A fragment encoding a FLAG tag and the ER exit signal of Kir2.1 (2) was cloned into the EcoRI and XbaI sites of pACU (2) by ligating with annealed oligos. The ATP8A coding region that is shared by all isoforms was amplified by PCR from cDNA clone GH28327 (AA26 to AA1091, BDGP) and inserted into an NheI site before the FLAG tag.

gRNA expression vectors: For *Nmnat*, *Sarm*, and *axed*, gRNAs were cloned into pAC-U63-tgRNA-Rev as described (3). The first tRNA spacer in each final construct is tRNA^{Gly} but the remaining tRNA spacers are tRNA^{Gln} (4). *gRNA-peb* and *gRNA-drpr* was constructed in pAC-U63-QtgRNA2.1-BR (4). The gRNA target sequences are listed in Table S2 .

The above constructs were injected by Rainbow Transgenic Flies to transform flies through φC31 integrase-mediated integration into attP docker sites.

CRISPR-TRiM

The efficiency of transgenic gRNA lines was validated by the Cas9-LEThAL assay (3). Homozygous males of each gRNA line were crossed to *Act-Cas9 w lig4* homozygous females. *gRNA-Nmnat* crosses caused lethality of all progeny at the 2nd instar larval stage; *gRNA-Sarm* crosses yielded viable female

progeny and male lethality between 3rd instar larvae to prepupae; *gRNA-axed* crosses caused lethality at the embryonic stage for all progeny; *gRNA-peb* crosses caused lethality from embryonic stage to the 2nd instar for all progeny; *gRNA-drpr* crosses resulted in lethality in late pupae. These results suggest that all gRNAs are efficient.

C4da-specific gene knockout was carried out using *ppk-Cas9* (3). Tissue-specific knockout in da neuron precursor cells were carried out with *SOP-Cas9* (3). Epidermis-specific knockout of *drpr* was induced by *shot-Cas9* (this study). Gene knockout in the precursor cells of Or22a ORNs was carried out using *ey-Cas9* (this study).

Live imaging

Animals were reared at 25°C in density-controlled vials (60-100 embryos/vial) on standard yeast-glucose medium (doi:10.1101/pdb.rec10907). Larvae at 125 hours AEL (wandering stage) or stages specified were mounted in 100% glycerol under coverslips with vacuum grease spacer and imaged using a Leica SP8 microscope equipped with a 40X NA1.30 oil objective. Larvae were lightly anesthetized with isoflurane before mounting. For consistency, we imaged dorsal ddaC neurons from A1-A3 segments (2-3 neurons per animal) on one side of the larvae. Unless stated otherwise, confocal images shown in all figures are maximum intensity projections of z stacks encompassing the epidermal layer and the sensory neurons beneath, which are typically 8–10 μm for 3rd instar larvae.

Injury assay

Injury assay at the larval stage was done as described previously (5). Briefly, larvae at 90 hr AEL were lightly anesthetized with isoflurane, mounted in a small amount of halocarbon oil under coverslips with grease spacers. The laser ablation was performed on a Zeiss LSM880 Confocal/Multiphoton Upright Microscope, using a 790 nm two-photon laser at primary dendrites of ddaC neurons in A1 and A3 segments. Animals were recovered on grape juice agar plates following lesion for appropriate times before imaging.

ORN axon injury assay was performed on 7-day-old male flies by removing the outer segments of both antennae as described in (6). The injured males were recovered for 7 days by transferring to fresh yeast-glucose medium every day. To examine Or22a axon degeneration, brains were dissected in PBST (0.2% Triton-X in PBS), fixed in 4% formaldehyde in PBS for 20 min, and then rinsed with PBST three times, 20 minutes each. Then the brains were mounted in SlowFade® Diamond Antifade Mountant (Thermo Fisher Scientific) and imaged using a Leica SP8 microscope with a 40x NA1.3 oil objective.

Long-term time-lapse imaging

Long-term time-lapse imaging at the larval stage was done as described previously (5, 7). Briefly, a layer of double-sided tape was placed on the coverslip to define the position of PDMS blocks. A small amount of UV glue was added to the groove of PDMS and to the coverslip. Anesthetized larvae were placed on top of the UV glue on the coverslip and then covered by PDMS blocks with the groove side contacting the larva. Glue was then cured by 365nm UV light. The coverslip with attached PDMS and larvae was mounted on an aluminum slide chamber that contained a piece of moisturized Kimwipes (Kimtech Science) paper. Time-lapse imaging was performed on a Leica SP8 confocal equipped with a 40x NA1.3 oil objective and a resonant scanner at digital zoom 0.75 and a 3-min or 2-sec interval. For imaging after ablation, larvae were pre-mounted in the imaging chamber and subjected to laser injury. The larvae were then imaged 0.5-1 hours after ablation. For calcium imaging before and immediately

after ablation, images were captured on a Zeiss LSM880 Confocal/Multiphoton Upright Microscope on which the ablation was performed.

Image analysis and quantification

Image processing and analyses were done in Fiji/ImageJ. Methods for tracing and measuring C4da neuron dendrite length have been previously described (1). Briefly, the images were segmented by Auto Local Threshold and reduced to single pixel skeletons before measurement of skeleton length by pixel distance. The dendrite debris measurement has been described previously (5). Briefly, a dendrite mask was first generated from projected images by Auto Local Threshold in order to create a region of interest (ROI) by dilation to map areas within one-epidermal-cell diameter (40 μm) from dendrites. Dendrite debris within the ROI was converted to binary masks based on fixed thresholds. Different thresholds were used for *ppk-C4-tdTom* and *ppk-Gal4 UAS-CD-tdTom* as they have different brightness. The dendrite pixel area (ADen), debris pixel area (ADeb), and ROI area (AROI) were measured and dendrite coverage ratio was calculated based on the following formula: 100·Adeb·AROI /(AROI- ADen)·ADen. For measuring Lact-GFP, two regions at empty epidermal regions were measured as background levels. TdTom signals on dendrites were used to generate dendrite masks for measurement of GFP within the masks. For kymographs, we used a custom macro based on the Straighten function to extract a strip of pixels centered at the selected dendrite branch. The maximum intensity pixel in the strip at each distance was used to generate a single-pixel line for each time frame. The final kymographs were displayed using the Fire lookup table (LUT).

Statistical Analysis

R was used to conduct statistical analyses and generate graphs. (*$p < 0.05$, **$p < 0.01$, and ***$p < 0.001$). Statistical significance was set at $p < 0.05$. Data acquisition and quantification were performed non-blinded. Acquisition was performed in ImageJ (batch processing for debris coverage ratio and fragmentation ratio, manually by hand for GFP-Lact binding) and Microsoft Excel. Statistical analyses were performed using R. We used the following R packages: car, stats, multcomp for statistical analysis and ggplot2 for generating graphs. Some graphs were made in Excel using its native plotting functions. For the statistical analysis we ran the following tests, ANOVA (followed by Tukey's HSD) when dependent variable was normally distributed and there was approximately equal variance across groups. When dependent variable was not normally distributed and variance was not equal across groups, we used Kruskal-Wallis (followed by Dunn's test, p-values adjusted with Benjamini-Hochberg method) to test the null hypothesis that assumes that the samples (groups) are from identical populations. To check whether the data fit a normal distribution, we generated qqPlots to analyze whether the residuals of the linear regression model is normally distributed. We used the Levene's test to check for equal variance within groups. The state of neuronal degeneration or fragmentation was compared using the Freeman-Halton extension of Fisher's exact test.

Replication

For all larval and adult imaging experiments, at least 3 biological replications were performed for each genotype and/or condition.

SI Figures

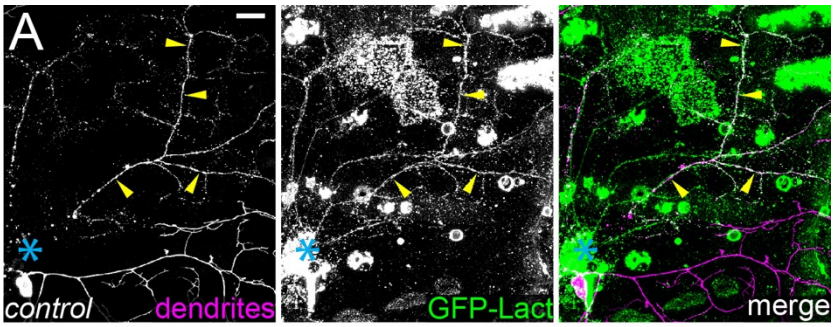

Figure S1: Injured dendrites expose PS

(A) GFP-Lact labeling on injured dendrites (yellow arrowheads) of a wildtype control C4da neuron at 5 hours AI.

Scale bar represents 20 µm. Blue asterisks indicate the injury site.

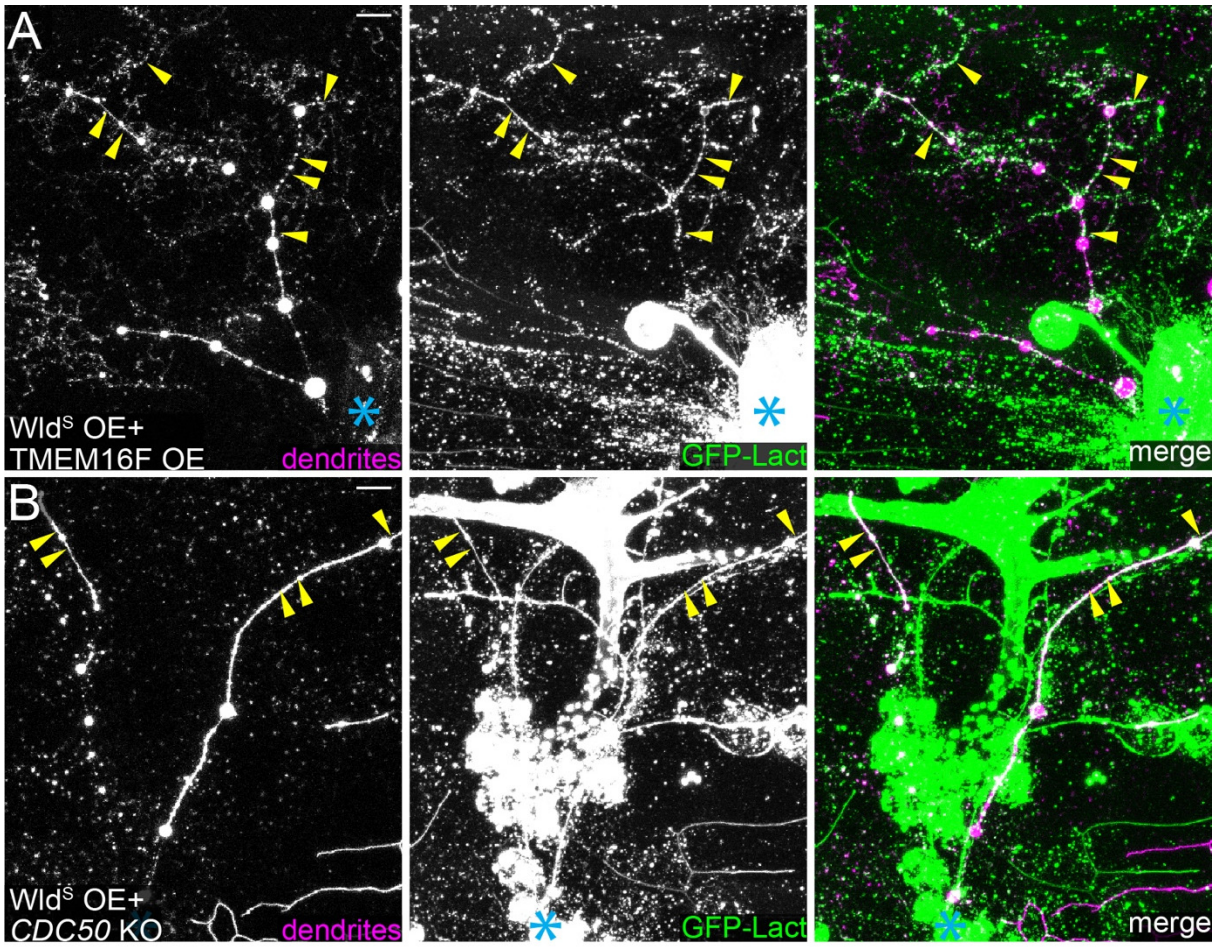

Figure S2: TMEM16F OE and *CDC50* KO causes ectopic PS exposure on injured dendrites of Wld^S OE neurons

(A) GFP-Lact labeling on injured dendrites (yellow arrowheads) of a Wld^S OE + TMEM16F OE neuron at 7 hours AI.

(B) GFP-Lact labeling on injured dendrites (yellow arrowheads) of a Wld^S OE + *CDC50* KO neuron at 6 hours AI.

Scale bars represent 10 μm (A and B). Blue asterisks indicate injury sites (A and B).

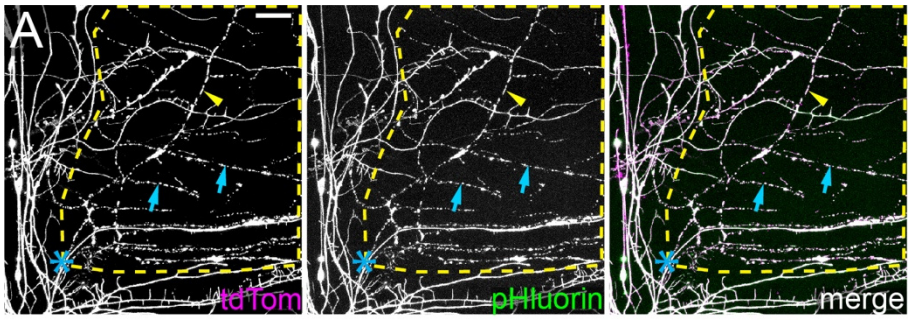

Figure S3: *drpr* KO in epidermal cells blocks engulfment of multiple classes of da neurons after injury

(A) Injured dendrites of a C1da (ddaE) neuron (cyan arrows) and a C4da (ddaC) neuron (yellow arrowhead) were not engulfed at 24 hours AI in epidermal KO of *drpr*. Dendrites of all da neurons were labeled by *RabX4-Gal4 UAS-MApHS*. Epidermis-specific *drpr* KO was induced by *shot-Cas9 gRNA-drpr*. The MApHS marker (8) consists of an extracellular pHluorin, a CD4 transmembrane domain, and an intracellular tdTom. Quenching of the pHluorin signal indicates engulfment, while the presence of both pHluorin and tdTom signals indicates the lack of engulfment. All injured dendrites fragmented but maintained pHluorin signals, indicating that injured dendrites were not engulfed.

The scale bar represents 25 μm. Blue asterisks indicate the injury sites. Yellow dash lines encircle regions covered by injured dendrites.

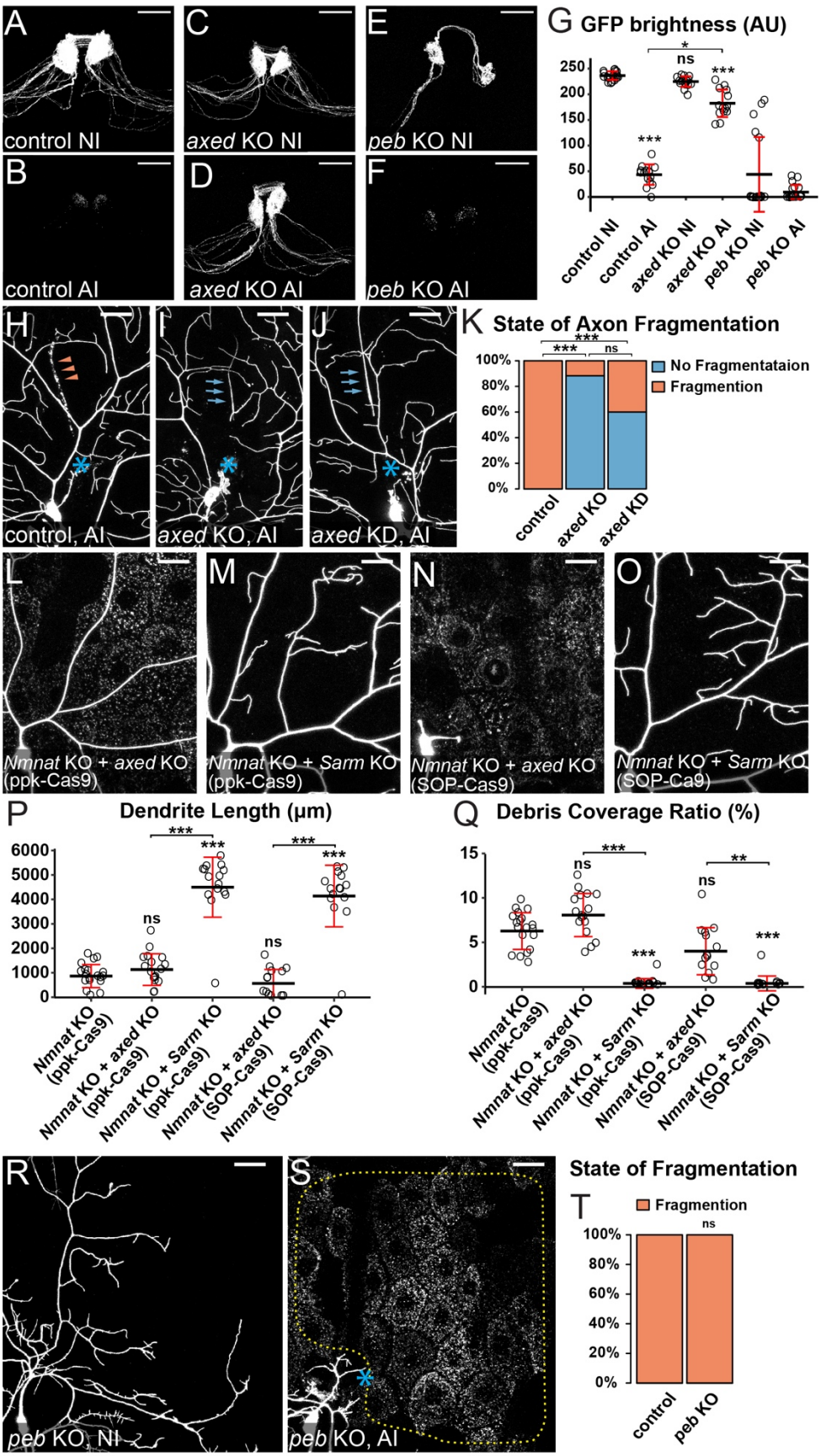
A
control NI
C
axed KO NI
E
peb KO NI
B
control AI
D
axed KO AI
F
peb KO AI
G GFP brightness (AU)
250
200
150
100
50
0
*
ns
***
***
control NI
control AI
axed KO NI
axed KO AI
peb KO NI
peb KO AI
H
control, AI
I
axed KO, AI
J
axed KD, AI
K State of Axon Fragmentation
***
***
ns
100%
80%
60%
40%
20%
0%
No Fragmentataion
Fragmention
control
axed KO
axed KD
L
Nmnat KO + axed KO (ppk-Cas9)
M
Nmnat KO + Sarm KO (ppk-Cas9)
N
Nmnat KO + axed KO (SOP-Cas9)
O
Nmnat KO + Sarm KO (SOP-Ca9)
P Dendrite Length (μm)
6000
5000
4000
3000
2000
1000
0
***
***
***
***
ns
ns
Nmnat KO (ppk-Cas9)
Nmnat KO + axed KO (ppk-Cas9)
Nmnat KO + Sarm KO (ppk-Cas9)
Nmnat KO + axed KO (SOP-Cas9)
Nmnat KO + Sarm KO (SOP-Cas9)
Q Debris Coverage Ratio (%)
15
10
5
0
***
**
ns
ns
***
***
Nmnat KO (ppk-Cas9)
Nmnat KO + axed KO (ppk-Cas9)
Nmnat KO + Sarm KO (ppk-Cas9)
Nmnat KO + axed KO (SOP-Cas9)
Nmnat KO + Sarm KO (SOP-Cas9)
R
peb KO, NI
S
peb KO, AI
State of Fragmentation
T
Fragmention
ns
100%
80%
60%
40%
20%
0%
control
peb KO

Figure S4: Axed is not involved in PS-mediated phagocytosis

(A-F) Axons of control NI (A), control 7 days AI (B), *axed* KO NI (C), *axed* KO 7 days AI (D), *peb* KO NI (E), and *peb* KO 7 days AI (F) Or22a neurons in 14-day-old adult brains. Or22a neurons were labeled by *Or22a>CD8-GFP* and KO was induced by *ey-Cas9*. Scale bars, 25 μm.

(G) Quantification of GFP brightness of Or22a glomeruli. n = number of brains: control NI 14 days (n = 19); control 7 days AI 14 days (n = 15); *axed* KO NI 14 days (n = 16); *axed* KO 7 days AI 14 days (n = 14); *peb* KO NI 14 days (n = 18); *peb* KO 7 days AI 14 days (n = 20). Kruskal-Wallis (One-way ANOVA on ranks) and Dunn's test, p-values adjusted with the Benjamini-Hochberg method. *p≤0.05, ***p<0.001, n.s., not significant. The significance level above each genotype is for comparison with the control. Statistical comparisons for *peb* KO glomeruli were not performed due to the variation within the group of *peb* KO NI 14 days. Black bar, mean; red bar, SD.

(H-J) Injured axons of wildtype 24 hrs AI (H), *axed* KO AI 24 hrs AI (I), and *axed* KD AI 24 hrs AI (J). Neurons were labeled by *ppk-MApHS*. Neuronal-specific KO was induced by *SOP-Cas9*, and neuronal-specific KD was driven by *21-7 Gal4*. Scale bars, 25 μm.

(K) Quantification of axon fragmentation showing percentages of neurons undergoing no fragmentation, and complete fragmentation of injured axons at 24 hrs AI. n = number of neurons: wildtype 24 hrs AI (n = 20, 12 animals); *axed* KO 24 hrs AI (n = 17, 9 animals); *axed* KD 24hrs AI (n = 20, 8 animals). Freeman-Halton extension of Fisher's exact test. For all quantifications, ***p≤0.001; n.s., not significant.

(L-O) Partial dendritic fields of *Nmnat* KO + *axed* KO (L and N) and *Nmnat* KO + *Sarm* KO (M and O) ddaC C4da neurons. Neurons were labeled by *ppk>CD4-tdTom* (L-O). The C4da-specific KO was induced by *ppk-Cas9* (L-M) or by *SOP-Cas9* (N-O). Scale bars, 25 μm.

(P) Quantification of dendrite length. n = number of neurons: *Nmnat* KO (*ppk-Cas9*) (n = 19, 10 animals); *Nmnat* KO + *axed* KO (*ppk-Cas9*) (n = 17, 9 animals); *Nmnat* KO + *Sarm* KO (*ppk-Cas9*) (n = 16, 8 animals); *Nmnat* KO + *axed* KO (*SOP-Cas9*) (n = 14, 7 animals); *Nmnat* KO + *Sarm* KO (*SOP-Cas9*) (n = 15, 8 animals). One-way ANOVA and Tukey's test.

(Q) Quantification of debris coverage ratio, which is the percentage of debris area normalized by dendrite area ratio. Number of neurons: same as in (P). Kruskal-Wallis (One-way ANOVA on ranks) and Dunn's test, p-values adjusted with the Benjamini-Hochberg method.

For all quantifications, **p≤0.01; ***p≤0.001; n.s., not significant. The significance level above each genotype is for comparison with the control. Black bar, mean; red bar, SD.

(R-S) Partial dendritic fields of *peb* KO NI (R) and *peb* KO 24 hrs AI (S) ddaC neurons. Yellow dots outline regions covered by injured dendrites in (S). Neurons were labeled by *ppk>CD4-tdTom* and neuronal-specific KO was induced by *SOP-Cas9*. Scale bars, 25 μm.

(T) Quantification of dendrite fragmentation showing percentages of neurons undergoing complete fragmentation of injured dendrites at 24 hrs AI. n = number of neurons: wildtype 24 hrs AI (n = 21, 12 animals); *peb* KO 24 hrs AI (n = 12, 7 animals). Freeman-Halton extension of Fisher's exact test. For all quantifications, n.s., not significant.

Figure S5: Membrane rupture assay on uninjured dendrites.

(A) Uninjured dendrites of a wildtype neuron that was laser-severed at another dendrite branch (injury site is outside the frame). The dendrites lacked reconstituted GFP signal. Scale bar, 10 μm.

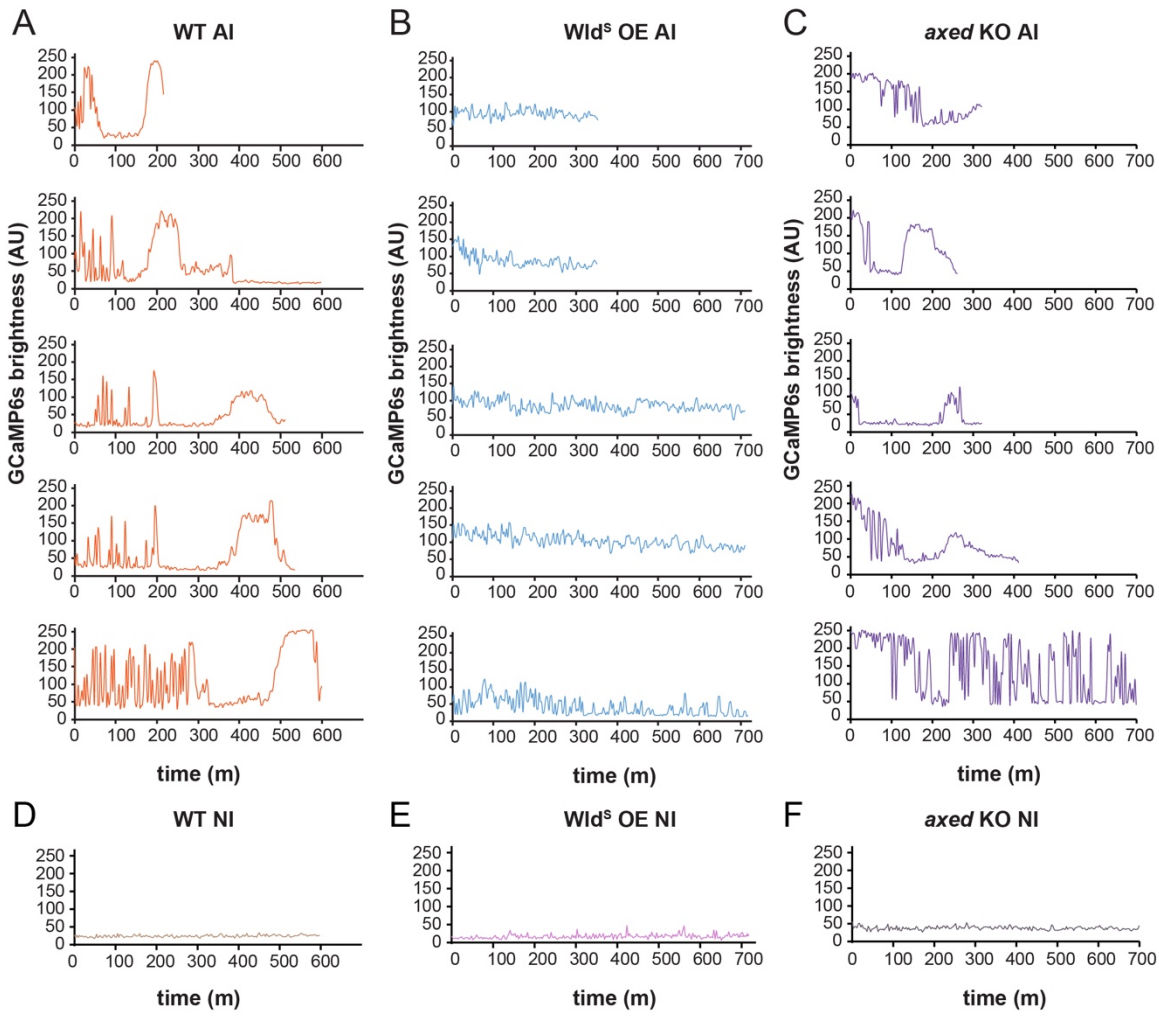

Figure S6: Wld^S overexpression and loss of *axed* changed calcium flashes in injured dendrites.

(A-C) Representative plots of GCaMP6s brightness in injured dendrites of wildtype (A), Wld^S-overexpressing (B), and *axed* KO (C) neurons over time with 3-min interval.

(D-F) Representative plots of GCaMP6s brightness in uninjured dendrites of wildtype (A), Wld^S-overexpressing (B), and *axed* KO (C) neurons over time with 3-min interval.

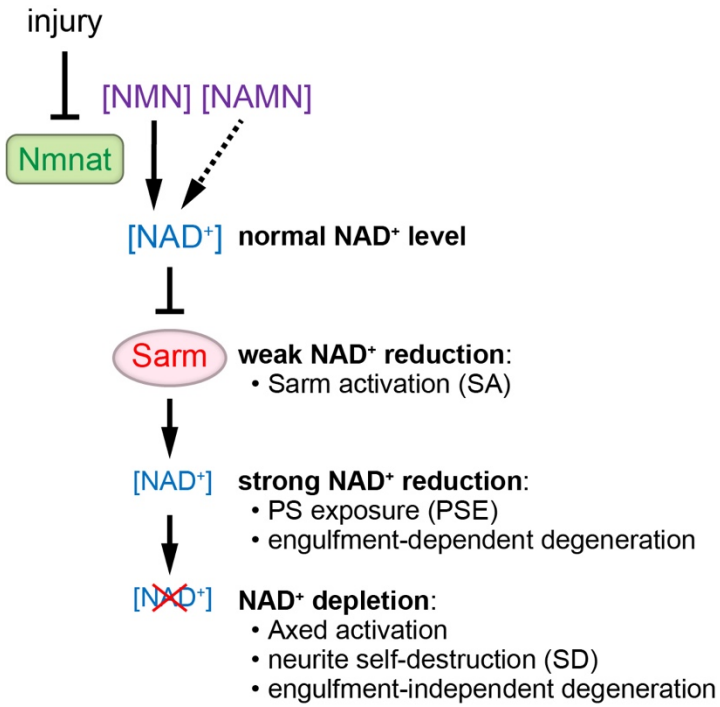

Figure S7. Potential roles of NAD^+ reduction in eliciting distinct responses in dendrites.
See Discussion for details.

SI Tables
Table S1. Key Resource Table.

REAGENT or RESOURCE	SOURCE	IDENTIFIER	ADDITIONAL INFORMATION
Experimental Models: Organisms/Strains			
ppk-Gal4	(9)		*ppk-Gal4^{VK00037}*
UAS-CD4-tdTom	(2)	RRID:BDSC_35841	*UAS-CD4-tdTom^{7M1}*
ppk-CD4-tdTom	(2)		*ppk-GFP(11)-CD4-tdTom^{2}*
ppk-Cas9	(3)		*ppk-Cas9^{7D}*
gRNA-Nmnat	this study		*gRNA-Nmnat^{VK00027}*
ppk-LexA	(1)		*ppk-LexA.GAD^{3}*
LexAop-Wld^{S}	this study		*LexAop-WldS^{VK00027}*
UAS-Wld$^{S\text{-}dead}$	(10)		
Sarm^{-}	(11)		*Sarm^{4705}*
Sarm^{-}	(11)		*Sarm^{4621}*
UAS-wnd	Bloomington Drosophila Stock Center	RRID:BDSC_51642	*UAS-wnd.C^{2}*
UAS-Cas9	Bloomington Drosophila Stock Center	RRID:BDSC_58986	*UAS-Cas9.P2^{attP2}*
drpr^{-}	(5)		*drpr^{indel3}*
UAS-JNK-RNAi	Bloomington Drosophila Stock Center	RRID:BDSC_57035	*TRiP.HMS04479^{attP40}*
Dcg-Gal4	(5)		
UAS-GFP-Lact	(5)		*UAS-GFP-LactC1C2^{VK00018}*
ppk-MApHS	(8)		*ppk-MApHS^{1}*
SOP-Cas9	(3)		*SOP-Cas9^{3A}*
gRNA-Sarm	this study		*gRNA-Sarm^{VK00027}*
R16A03-LexA	(5)		*R16A03-LexAp65^{VK00027}*
LexAop-GFP-LactC1C2	(5)		*LexAop2-GFP-LactC1C2^{VK00033}*
Or22a-Gal4	(6)		
UAS-mCD8-GFP	(6)		
ey-Cas9	this study		*ey-Cas9^{VK00005}*
gRNA-axed	this study		*gRNA-axed^{VK00027}*
gRNA-peb	this study		*gRNA-peb(BR)^{VK00027}*
gRNA-drpr	this study		*gRNA-drpr(BR)^{VK00027}*

R38F11-Gal4	Bloomington Drosophila Stock Center	RRID:BDSC_50014	*R38F11-Gal4^{attP2}*
shot-Cas9	this study		
RabX4-Gal4	Bloomington Drosophila Stock Center	RRID:BDSC_51602	*RabX4-Gal4.ORF(loxP)^{VK00033}; 3xP3-RFP was removed*
UAS-MApHS	(8)		*UAS-MApHS^{VK00019}*
UAS-TMEM16F	(5)		*UAS-TMEM16F(D430G)^{VK00016}*
UAS-Wld^{S}	(6)		
gRNA-CDC50	(5)		*gRNA-CDC50^{attP2}*
Df(drpr)	Bloomington Drosophila Stock Center	RRID:BDSC_9693	*Df(3L)BSC181*
UAS-SarmGOF	(12)		*UAS-Sarm$^{\Delta Arm}$*
UAS-JNK^{DN}	Bloomington Drosophila Stock Center	RRID:BDSC_6409	*UAS-bsk.DN^{2}*
LexAop-myr-tdTom-GFP(1-10)	this study		*LexAop2-myr-tdTom-GFP(1-10)^{VK00005}*
UAS-sGFP(11)x7	this study		*UAS-sGFP(11)x7^{VK00027}*
LexAop-myr-GCaMP6s	(13)		*13xLexAop2-myr::GCaMP6s*
Gal4$^{21-7}$	(14)		
UAS-AnnexinV-mCard	(5)		*UAS-AnnexinV-mCard^{VK00037}*
Recombinant DNA			
pJFRC176-10XUAS-rox-dSTOP-rox-myr-GFP	Addgene	RRID:Addgene_32147	
pAC-U63-tgRNA-Rev	(3)	RRID:Addgene_112811	
pAC-U63-QtgRNA2.1-BR	(4)	RRID:Addgene_170513	
pIHEU-sfGFP-LactC1C2	(5)		
pAPLO-CD4-tdTom	(1)		
pDEST-APIC-Cas9	(3)	RRID:Addgene_121657	
pENTR11	Thermo Fisher Scientific	#A10467	
Software and Algorithms			
Fiji	https://fiji.sc/	RRID: SCR_002285	

R	https://www.r-project.org/	RRID: SCR_001905	
Adobe Photoshop	Adobe	RRID:SCR_014199	
Adobe Illustrator	Adobe	RRID:SCR_010279	
Other			
Gateway™ LR Clonase™ II Enzyme mix	Thermo Fisher Scientific,	#11791020	
NEBuilder® HiFi DNA Assembly Master Mix	New England Biolabs Inc.	#E2621	

Table S2. gRNA target sequences.

Gene	Target sequence 1	Target sequence 2
Sarm	GCATCTGTTCAAACACTCCG	CGATTCCAATATCAGCCCGG
Nmnat	GGAACCCACAGAGTGGTAGG	TAAGAGCCGCCGAATCAACG
axed	GTCGGTACTCGAGCGGAGCG	TGGACCCGATGGCCATCACG
peb	ATTTCGTCTGAATCGCTCGG	ACGCATGTGACGCACCAGGG
drpr	CCATGCCGTAGAATCCAGGT	ACGGACAAGGATGCGCCCAG

SI Video Legends

Video S1 (separate file). GFP-Lact labeling of degenerating *Nmnat* KO dendrites, related to Figure 2.

Time-lapse movie of GFP-Lact labeling on distal dendrites of a *Nmnat* KO C4da neuron before and during degeneration. Imaging started around 96 hours AEL. *Dcg-Gal4* drives GFP-Lact expression in both fat bodies and hemocytes (mobile cells in the GFP-Lact channel). Timestamp is relative to the first frame, with a 3-min interval between each frame.

Video S2 (separate file). Dendrite dynamics of *Nmnat* KO neurons in *drpr* mutant larvae, related to Figure 2.

Time-lapse movie of dendrites of a *Nmnat* KO neuron exhibiting dynamic extension and retraction behaviors in a *drpr* mutant larva. Imaging started around 120 hours AEL. Timestamp is relative to the first frame, with a 3-min interval between each frame.

Video S3 (separate file). Cytoplasmic calcium dynamics in uninjured wildtype dendrites, related to Figure 8.

Time-lapse movie of an uninjured wildtype C4da neuron showing low baseline GCaMP6s signals and occasional local rises in dendrites. Timestamp is relative to the first frame, with a 3-min interval between each frame.

Video S4 (separate file). Cytoplasmic calcium dynamics in dendrites of *Nmnat* KO neurons, related to Figure 8.

Time-lapse movie of a *Nmnat* KO C4da neuron showing calcium dynamics in uninjured dendrites. Timestamp is relative to the first frame, with a 3-min interval between each frame.

Video S5 (separate file). Calcium dynamics in injured wildtype dendrites, related to Figure 8.

Time-lapse movie of laser-injured C4da dendrites from 1 to 11 hrs AI showing calcium dynamics in both severed dendrites and those attached to the soma. Timestamp is relative to the first frame, with a 3-min interval between each frame.

Video S6 (separate file). AV-mCard labeling and calcium dynamics of injured dendrites, related to Figure 8.

Time-lapse movie of laser-injured C4da dendrites from 1 to 6 hrs AI showing labeling of injured dendrites by the PS sensor AV-mCard and GCaMP6s signals. Timestamp is relative to the first frame, with a 3-min interval between each frame.

Video S7 (separate file). Calcium dynamics in injured Wld^S OE dendrites, related to Figure 8.

Time-lapse movie of laser-injured Wld^S OE C4da dendrites from 1 to 13 hours AI showing GCaMP6s signals in severed dendrites. Timestamp is relative to the first frame, with a 3-min interval between each frame.

Video S8 (separate file). Calcium dynamics in injured wildtype dendrites with a higher temporal resolution, related to Figure 8.

High temporal-resolution time-lapse movie of laser-injured wildtype C4da dendrites around 1 hr AI showing calcium dynamics. Timestamp is relative to the first frame, with a 2-sec interval between each frame.

Video S9 (separate file). Calcium dynamics in injured Wld^S OE dendrites at a higher temporal resolution, related to Figure 8.

High temporal-resolution time-lapse movie of laser-injured Wld^S OE C4da dendrites around 2 hrs AI showing calcium dynamics. Timestamp is relative to the first frame, with a 2-sec interval between each frame.

Video S10 (separate file). Irregular and infrequent cytoplasmic calcium flashes in injured Wld^S OE dendrites at a higher temporal resolution, related to Figure 8.

High temporal-resolution time-lapse movie of laser-injured Wld^S OE C4da dendrites around 2 hrs AI showing irregular and infrequent GCaMP6s signals in severed dendrites. Timestamp is relative to the first frame, with a 2-sec interval between each frame.

Video S11 (separate file). Calcium dynamics in injured *axed* KO dendrites, related to Figure 8.

Time-lapse movie of laser-injured *axed* KO C4da dendrites from 0.5 to 5.5 hours AI showing GCaMP6s signals in severed dendrites. Timestamp is relative to the first frame, with a 3-min interval between each frame.

Video S12 (separate file). Calcium dynamics in injured *axed* KO dendrites at a higher temporal resolution, related to Figure 8.

High temporal-resolution time-lapse movie of laser-injured *axed* KO C4da dendrites around 10 min AI showing calcium dynamics. Timestamp is relative to the first frame, with a 2-sec interval between each frame.

SI References

1. Poe AR*, et al.* (2017) Dendritic space-filling requires a neuronal type-specific extracellular permissive signal in Drosophila. *Proc Natl Acad Sci U S A* 114(38):E8062-E8071.
2. Han C, Jan LY, & Jan YN (2011) Enhancer-driven membrane markers for analysis of nonautonomous mechanisms reveal neuron-glia interactions in Drosophila. *Proc Natl Acad Sci U S A* 108(23):9673-9678.
3. Poe AR*, et al.* (2019) Robust CRISPR/Cas9-Mediated Tissue-Specific Mutagenesis Reveals Gene Redundancy and Perdurance in Drosophila. *Genetics* 211(2):459-472.
4. Koreman GT*, et al.* (2021) Upgraded CRISPR/Cas9 tools for tissue-specific mutagenesis in Drosophila. *Proc Natl Acad Sci U S A* 118(14).
5. Sapar ML*, et al.* (2018) Phosphatidylserine Externalization Results from and Causes Neurite Degeneration in Drosophila. *Cell Rep* 24(9):2273-2286.
6. MacDonald JM*, et al.* (2006) The Drosophila cell corpse engulfment receptor Draper mediates glial clearance of severed axons. *Neuron* 50(6):869-881.
7. Ji H & Han C (2020) LarvaSPA, A Method for Mounting Drosophila Larva for Long-Term Time-Lapse Imaging. *J Vis Exp* (156).
8. Han C*, et al.* (2014) Epidermal cells are the primary phagocytes in the fragmentation and clearance of degenerating dendrites in Drosophila. *Neuron* 81(3):544-560.

9. Han C*, et al.* (2012) Integrins regulate repulsion-mediated dendritic patterning of drosophila sensory neurons by restricting dendrites in a 2D space. *Neuron* 73(1):64-78.

10. Avery MA, Sheehan AE, Kerr KS, Wang J, & Freeman MR (2009) Wld S requires Nmnat1 enzymatic activity and N16-VCP interactions to suppress Wallerian degeneration. *J Cell Biol* 184(4):501-513.

11. Osterloh JM*, et al.* (2012) dSarm/Sarm1 is required for activation of an injury-induced axon death pathway. *Science* 337(6093):481-484.

12. Neukomm LJ*, et al.* (2017) Axon Death Pathways Converge on Axundead to Promote Functional and Structural Axon Disassembly. *Neuron* 95(1):78-91 e75.

13. Akbergenova Y, Cunningham KL, Zhang YV, Weiss S, & Littleton JT (2018) Characterization of developmental and molecular factors underlying release heterogeneity at Drosophila synapses. *Elife* 7.

14. Song W, Onishi M, Jan LY, & Jan YN (2007) Peripheral multidendritic sensory neurons are necessary for rhythmic locomotion behavior in Drosophila larvae. *Proc Natl Acad Sci U S A* 104(12):5199-5204.